View metadata, citation and similar papers at core.ac.uk
brought to you by CORE
provided by CURVE/open

Realization of High Efficiency and Low Damage Machining of Anisotropic KDP Crystal by Grinding

Qu, M., Jin, T. & Cai, R.

Author post-print (accepted) deposited by Coventry University's Repository

Original citation & hyperlink:
Qu, M, Jin, T & Cai, R 2018, 'Realization of High Efficiency and Low Damage Machining of Anisotropic KDP Crystal by Grinding' Precision Engineering, vol. (In-Press), pp. (In-Press).
https://dx.doi.org/10.1016/j.precisioneng.2018.10.016

DOI 10.1016/j.precisioneng.2018.10.016
ISSN 0141-6359

Publisher: Elsevier

NOTICE: this is the author's version of a work that was accepted for publication in *Precision Engineering*. Changes resulting from the publishing process, such as peer review, editing, corrections, structural formatting, and other quality control mechanisms may not be reflected in this document. Changes may have been made to this work since it was submitted for publication. A definitive version was subsequently published in *Precision Engineering,* 2018 DOI:10.1016/j.precisioneng.2018.10.016

© 2017, Elsevier. Licensed under the Creative Commons Attribution-NonCommercial-NoDerivatives 4.0 International http://creativecommons.org/licenses/by-nc-nd/4.0/

Copyright © and Moral Rights are retained by the author(s) and/ or other copyright owners. A copy can be downloaded for personal non-commercial research or study, without prior permission or charge. This item cannot be reproduced or quoted extensively from without first obtaining permission in writing from the copyright holder(s). The content must not be changed in any way or sold commercially in any format or medium without the formal permission of the copyright holders.

This document is the author's post-print version, incorporating any revisions agreed during the peer-review process. Some differences between the published version and this version may remain and you are advised to consult the published version if you wish to cite from it.

Realization of High Efficiency and Low Damage Machining of Anisotropic KDP Crystal by Grinding

Meina Qu [a, b], Tan Jin [a, b,], Rui Cai [c], Ange Lu [a, b]

[a] National Engineering Research Centre for High Efficiency Grinding, Hunan University, Changsha, Hunan 410082, China

[b] College of Mechanical and Vehicle Engineering, Hunan University, Changsha, Hunan 410082, China

[c] Mechanical, Automotive and Manufacturing (MAM) Faculty of Engineering Environment and Computing, Coventry University, 3 Gulson Road, Coventry, CV1 2JH, UK

[1] Corresponding author. Tel.: +86 731 88821833; fax: +86 731 88823921. E-mail address: tjin@hnu.edu.cn

Realization of High Efficiency and Low Damage Machining of Anisotropic KDP Crystal by Grinding

Abstract: Potassium dihydrogen phosphate (KDP) is a non-linear crystal material used in various opto-electronic applications including Q-switches, high-speed photography shutters, frequency harmonic generation lens and Pockels cells in the Inertial Confinement Fusion (ICF) devices. KDP belongs to the most difficult-to-cut material, due to its delicate and unique characteristics including the combination of softness with brittleness, anisotropic performances, tendency for deliquescence and sensitivity to temperature change. Single point diamond turning (SPDT) is considered to be the ideal method for machining of KDP components. However, the process efficiency is rather low and often accompanied with severe tool wear issues. This paper studies the feasibility using grinding method to remove the surface material of KDP components with high process efficiency and low damage, fulfilling the task of re-aligning the surface orientation to the crystalline axis. The direction of precision grinding was determined by studying the anisotropy of KDP, including its elastic modulus E, Vickers hardness H_V and fracture toughness K_{IC}, to reduce the influence of material anisotropy on machining quality. The grinding tests are carried out on a common CNC grinder, using resin bonded diamond grinding wheel, whilst the diamond abrasives are coated with Ni-P alloy. The grinding process parameters were preliminarily determined based the experimental results investigating the effects of spindle speed, worktable feed rate and grinding depth on the ground surface roughness. The surface morphology, surface defects and sub-surface damage under different process parameters were investigated. Surface roughness $R_a \leq 0.3$µm and sub-surface damage depth SSD≤6µm were obtained. The machining efficiency can be improved by

nearly ten times using the proposed precision grinding method, producing nearly the same surface quality(R_a≤0.2μm, SSD≤6μm) as that in the axis fixed phase by SPDT.

Keywords: KDP crystal High efficiency Low damage Grinding Crystal axis fixed

1. Introduction

KDP is a non-linear opto-electronic crystal. It is widely used in sonar and piezoelectric products, Q-switches, high speed photography shutters, electro-optical modulators, and frequency harmonic generation lens. Large size KDP crystal components with high surface form accuracy are required for making the Pockels cells in the Inertial Confinement Fusion (ICF) devices [1]. KDP is believed to be the most difficult-to-cut material, due to its delicate and unique characteristics including the combination of softness with brittleness, anisotropic performances, tendency for deliquescence and sensitivity to temperature change [2, 3]. Long process time is typically required for the complete machining of ultra-precision KDP components, covering sawing [4], correction of crystal axis [5], chamfering [6] and ultra-precision machining [7, 8].

According to previous studies, single point diamond turning (SPDT) or fly-cutting technique is the ideal method for the precision machining of KDP components. High-end machine tools at ultra precision level are required to carry out the diamond machining processes, using single crystal diamond cutters with extreme sharpness to remove very thin layers of work-piece surface material [9]. Fuchs et al. produced

finished KDP parts on an modified Moore lathe with no need for additional surface polishing, with component surface roughness better than 8-Å RMS and 36-Å P-V. However, the process efficiency for removing the top surface material and to align the surface orientation to the crystalline axis was very low, using cross-feed rate at only 19.1 mm/min and cutting depth 20μm [5]. Namba, et al. achieved super smooth surface of RMS 1.09nm on a KDP test piece, using a single point diamond tool with rake angle -25°and nose radius 1mm, on an ultra-precision diamond turning machine, under the process parameters of cutting speed of 500m/min, feed 2μm/rev and depth of cut 1μm [10]. Chen et al. designed an ultra-precision fly cutting machine tool with a gantry type structure for KDP crystal machining, which is equipped with a high-speed spindle and shows an excellent slow-feed performance, whilst a diamond cutter with a large nose radius is adopted [11]. The consequence of using the SPDT process, which is a typical ultra-precision machining method, to remove the large amount of KDP surface allowance material, would result in rather slow process efficiency often accompanied with severe tool wear issues [12].

Compared with SPDT, grinding method is also suitable as a process for aligning the KDP surface orientation to the crystalline axis, with potential advantages including higher process efficiency, better process stability with no tool breakage and possibly no surface waviness or ripples when using a flat cup wheel. Namba carried out grinding tests on a ultra-precision grinder developed in their laboratory using resin bonded

diamond wheel and produced super-smooth surface on KDP crystal with surface roughness 0.553nm (RMS), 0.441 nm (Ra) and 3.40nm(PV), whilst details regarding the process design was not reported [13]. Wang et al. conducted preliminary study on the precision grinding of KDP crystals on a horizontal surface grinder, using resin bonded diamond wheel, and effects of machining parameters on grinding force and surface roughness were investigated. However, the influence of material anisotropy was not considered, and effects of grinding process on the sub-surface damage of KDP work-pieces were not investigated, which is an important issue for evaluating the feasibility of the grinding process [14]. Chen et al. proposed a hybrid machining method by combining precision grinding with fly cutting and achieved nearly five times machining efficiency [15].

The present paper systematically studied the feasibility using grinding method to remove the surface material of KDP components with high process efficiency and low surface and sub-surface damages conducted on a common CNC grinder, using a resin bonded grinding wheel with Ni-P coated diamond abrasives. In this context, the anisotropy of elastic modulus E, Vickers hardness H_V and fracture toughness K_{IC} were used to determine the grinding direction. Here, the effects of spindle speed, worktable feed rate and grinding depth on the ground surface roughness were investigated. Surface morphology and defects, sub-surface damage (SSD) and machining efficiency were contrasted to SPDT.

2. Materials and methods

2.1 KDP crystal samples

The grinding tests were conducted on the sample surfaces parallel to the (001) plane of KDP crystal, the sample size is 20mm×20mm×10mm. As KDP belongs to a tetragonal crystal system with a single crystal axis, it only needs to measure and calculate the mechanical anisotropy within the range of 0°~90° around the crystal axis. The crystal surfaces were checked using X-ray crystal orientation analyzer, making sure the deviation of surface orientation is less than 6. The samples were carefully polished to obtain smooth surfaces with roughness (R_a) less than 5nm before micro-Vickers indentation tests.

2.2 The anisotropy of E, H_V and K_{IC}

The directional distribution of the elastic modulus E, micro-hardness H_V, and especially the fracture toughness K_{IC} of the KDP crystal on the (001) surface provides important information for selecting the appropriate grinding direction, as micro-fracture is the dominant mechanism of KDP material removal [16].

The elastic modulus E in different angular direction on the (001) crystal plane can be calculated using the anisotropic structural mechanics theory [17], as shown below. The values of flexibility coefficients used in the calculation are shown in Table 1[18].

$$\frac{1}{E} = S_{11}\left(a^4 + b^4\right) + S_{33}g^4 + \left(2S_{13} + S_{44}\right)\left(a^2 + b^2\right)g^2 + \left(2S_{12} + S_{66}\right)a^2b^2 \quad (1)$$

$$a = \frac{h}{\sqrt{h^2 + k^2 + l^2}} \tag{2}$$

$$b = \frac{k}{\sqrt{h^2 + k^2 + l^2}} \tag{3}$$

$$g = \frac{l}{\sqrt{h^2 + k^2 + l^2}} \tag{4}$$

$$\frac{1}{E_{(001)}} = S_{11} + \left(2S_{12} + S_{66} - 2S_{11}\right)\left(\sin\theta\cos\theta\right)^2 \tag{5}$$

where a is the direction cosine relative to the x-axis; b is the direction cosine relative to the y-axis; g is the direction cosine relative to the z-axis; [h k l] represents a crystal in the one crystal orientation; S_{ij} is the flexibility coefficient;

Table 1. Flexibility coefficients (Unit: GPa)

S_{11}	S_{12}	S_{13}	S_{33}	S_{44}	S_{66}
151	18	-40	195	781	1620

Variation of Vickers hardness in the range of 0°~90° around the crystal axis, on the sample surface, i.e., the (001) plane, were measured using micro-indentation instrument. Measurements under different loads, P (0.5N, 1N, 2N, 3N), were conducted along the x-axis direction, to determine the suitable load level generating sufficient indentation size and depth, a and c, and relatively low level of fracture cracks. Load level P=1N, was selected in the following measurements at different angular positions (15° interval)，as shown in Fig. 3a. The indenter was kept for 10 seconds under the load on the sample surface before unloading. For each angular position, six measurements along the radial direction were conducted to obtain the average hardness value at this position.

The variation of fracture toughness K_{IC} was calculated according to the model proposed by Anstis, as shown below [19], using the calculated elastic modulus E and measured Vickers hardness H_V values.

$$K_{IC} = (0.016 \pm 0.004)\left(\frac{E}{H_v}\right)^{1/2} \frac{P}{c^{3/2}} \tag{6}$$

where c is half the length of radial crack. a is half of the diagonal length. When using the Anstis model, the load P, indentation size a and radial crack length c need to meet the conditions: (1) P and $c^{3/2}$ satisfy linear relationship; (2) $c/a > 2.5$.

2.3 Precision grinding experiments

2.3.1 Grinding machine

Grinding experiments were carried out on a MK2945C high-precision CNC grinding machine. The grinding machine has six movement control axes (*X, Y, Z, C, A, U*). For *X, Y, C* and *A* axis, any three axes can be simultaneously controlled to generate 3-axis movements. *X* and *Y* axis adopt closed loop control using HEIDENHAIN grating rulers; the movement control resolution is 0.1 μm. Because servo-motor is used to control Z-axis, tolerance on down reversing point is within 0.05mm, the movement resolution is 0.1 μm. In addition, the grinding head power is up to 1KW.

2.3.2 Grinding wheel and dressing

According to physical and mechanical properties, a resin bond diamond cup wheel, with average abrasive grit size 35μm, was used in the present research (Table 2). The

diamond abrasives on the wheel are coated with Ni-P alloy, as shown in Fig. 1. The Ni-P alloy coating helps to enhance the interfacial bonding between the diamond abrasives and resin bond and also increase the strength of abrasives, which are beneficial to avoid abrasives pulling out from the wheel and stabilize the grinding performance of the wheel [20].

The grinding wheel was dressed using a silicon carbide roller. The face runout of the wheel after dressing is about 10μm and the average protrusion height of the abrasives is about 12μm.

Table 2. Parameters of grinding wheel

Diameter, D	50mm
Abrasive layer width, W	7mm
Binder hardness	Medium hardness resin bond
Substrate material	Aluminum alloy
Concentration, C	100%

2.3.3 Grinding condition and parameters

To eliminate the potential effects of grinding fluids, the grinding tests were conducted under dry grinding condition.

To find out the suitable grinding parameters, preliminary tests were carried out, investigating the effects of spindle speed, worktable feed rate and grinding depth on the ground surface roughness Ra, grinding parameters used are listed in Table 3. The schematic diagram of the grinding test setup is shown in Fig. 1.

Table 3. Grinding parameters in initial tests

spindle speed（r/min）	3000、4000、5000、6000、7000
worktable feed rate (mm/min)	60、90、120、150、180、210、240

grinding depth（μm）	2、4、6、8、10、12、14、16、18、20、22、24

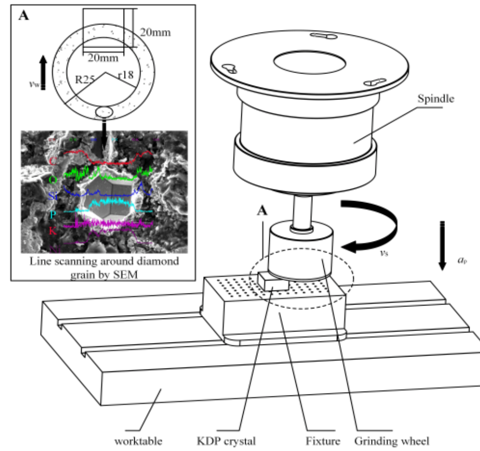

Fig. 1 Schematic diagram of grinding test setup

2.4 Testing equipment and methods

2.4.1 Surface roughness

A high-resolution laser roughness measurement instrument (Laser-check), was used to measure the ground surface roughness, R_a. The instrument measurement range of R_a is 0.01-10 μm, with a repetitive accuracy ±3%. Measurements of the ground surface roughness on each sample were repeated 10 times to obtain the average roughness value under a certain grinding test condition.

2.4.2 Surface geomorphology and defects

The ground sample surfaces were observed under a 3D optical microscope (VHX-1000, KEYENCE, resolution: 5800 pixels, depth of field: up to 10 mm, magnification: 20~5000 times). Before the observation, the ground samples were cleaned in anhydrous alcohol. Scanning electron microscope (SEM) and energy dispersive spectroscopy (EDS) were also used in the present research to identify the surface defects.

2.4.3 Subsurface damage

Typical techniques used to expose the sub-surface damage under the ground surface include cross section polishing, taper polishing and ball dimpling polishing. Level of SSD at selected locations can be evaluated using these methods. In the present work, layer by layer polishing technique is adopted, which enables thorough evaluation of SSD on the overall ground surface and avoids the possibility of under or over-estimate the SSD due to the improper selection of locations. The sample preparation and observation procedures are as follows: (i) polish the sample surface using an oil-based aluminum oxide polishing liquid on a polishing machine; (ii) put the polished sample into waterless alcohol and then wipe the sample with clean cloth very gently, pay attention not to introduce new scratches; (iii) observe the surface under 3D optical microscope. The top surface material is removed layer by layer and observed under microscope following the steps above, until there are no cracks and other sub-surface damages in the observed images.

3. Results

3.1 Directional variations of elastic modulus E, Vickers hardness H_V and fracture toughness K_{IC}

Calculated values of elastic modulus E, at different angular positions are shown in Fig. 2a. The maximum elastic modulus value (66.2 GPA) is located at 0° and 90°, whilst the minimum value (20.4 GPA) is at 45°. Fig. 3b shows a group of indentations under 1N load obtained from the micro-hardness measurements. The diagonal lengths of the

indentations and lengths of maximum lateral cracks (equivalent to radial cracks) were estimated to evaluate the Vickers hardness values. Variation of the Vickers hardness along the crystal orientation 0° and 90° is shown in Fig. 2b.

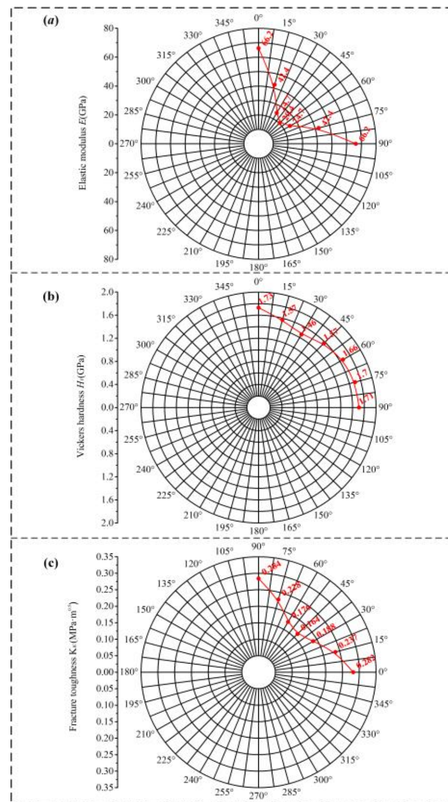

Fig. 2 Directional variations of (a) Elastic modulus, (b) Micro Vikers hardness and (c) Fracture toughness

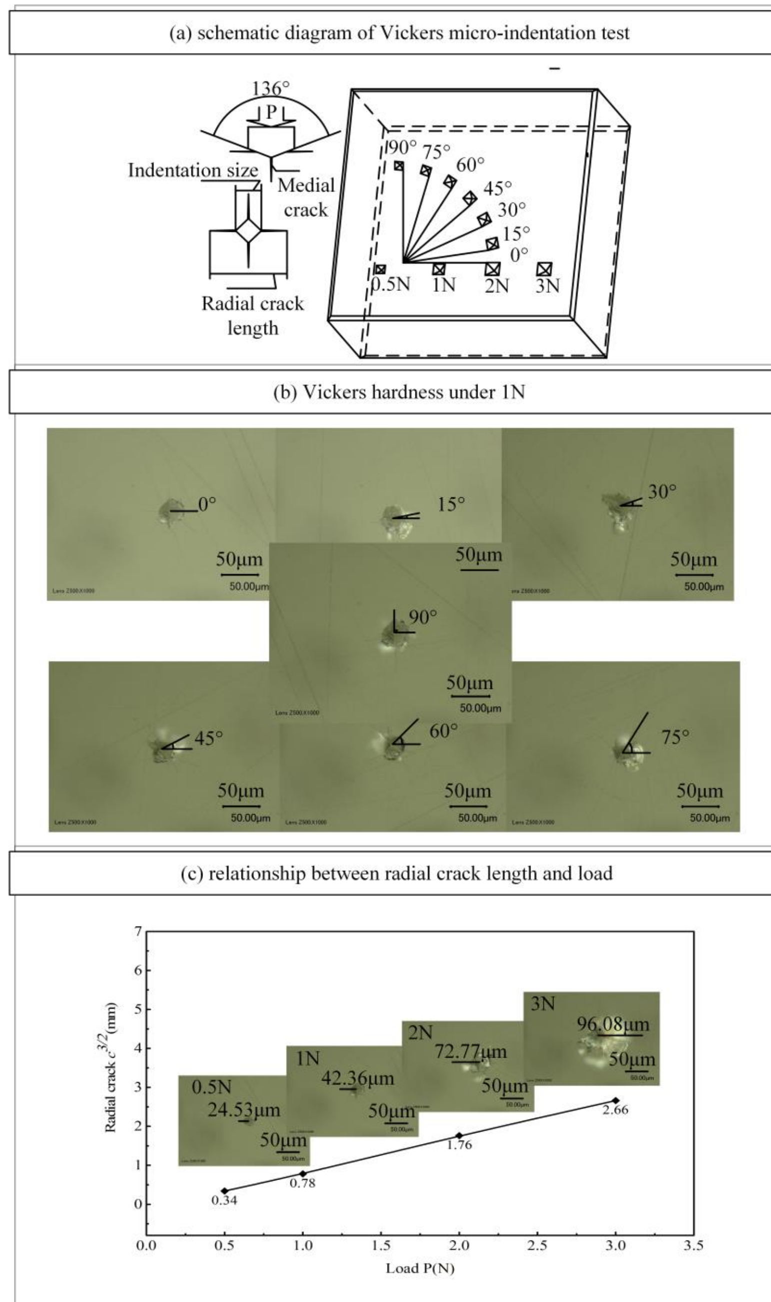

Fig. 3 Micro-indentation measurements: (a) schematic diagram of Vickers micro-indentation test (b) Vickers hardness under 1N (c) relationship between radial crack length and load

There are several models available to calculate the fracture toughness. The appropriate selection of the model depends on the relations of $P/c^{3/2}$ and c/a. Under different load 0.5N, 1N, 2N and 3N, Anstis model requires that the average value of $P/c^{3/2}$ needs to be close to a constant, and c/a needs to be more than 2.5, Fig. 3c shows

the relation between radial crack length and lower indenting loads. Variation of the fracture toughness K_{IC} is shown in Fig. 2c. The maximum the fracture toughness is at 0° and 90°, whilst the minimum value is at 45°. The anisotropic difference of K_{IC} is 42.3%. The measurement results are consistent with those obtained by Zhang et al [21]. in the study of slip system of KDP crystal.

3.2 Effects of grinding parameters on the surface roughness

According to the influence of grinding parameters on the surface roughness can help to determine the suitable process parameters for the precision grinding of KDP crystal conveniently, because surface roughness Ra measured easily and has a certain connection on sub-surface damage[21].

3.2.1 Influence of spindle speed on surface roughness

As shown in Fig. 4a, the surface roughness R_a increased slightly with the increase of spindle speed, when the spindle speed is less than 5000rpm. The variation of ground surface roughness followed a downward trend with the increase of wheel speed, when the spindle speed is higher than 5000rpm. Considering the process stability and machining efficiency, spindle speed 7000rpm would be suitable for the grinding of KDP samples.

3.2.2 Influence of worktable feed rate on surface roughness

As shown in Fig. 4b, the worktable feed rate had little effect on the ground surface roughness when it was less than 120mm/min. Further increase of worktable feed rate,

produced obvious increase of the surface roughness. However, the ground samples edge breakages became more serious when the worktable feed rate was greater than 240mm/min. 210 mm/min can be selected as a reasonable machine tool feed rate.

3.2.3 Influence of grinding depth on surface roughness

The measured ground surface roughness R_a showed a strong dependence with the grinding depth a_p, as shown in Fig. 4c. Based on the test results, the process parameters for the precision grinding of KDP crystal were preliminarily selected, as shown in Table 4.

Table 4. Grinding process parameters

Spindle speed n (r/min)	Worktable feed rate V_W (mm/min)	Grinding depth a_p (μm)
7000	210	20
7000	210	10
7000	210	2

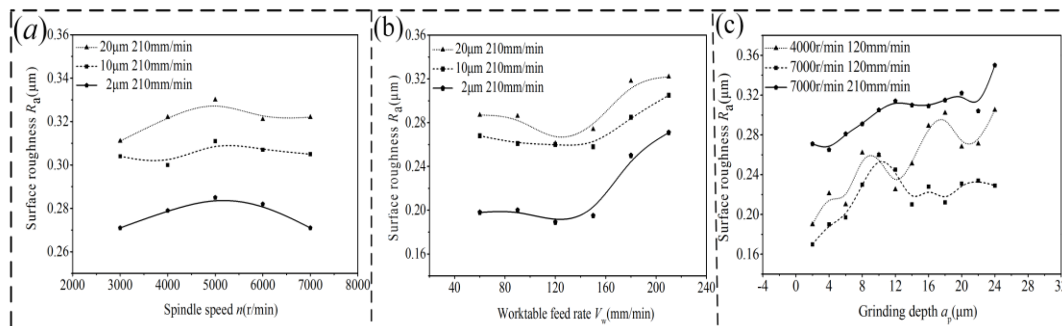

Fig. 4 Effects of grinding parameters on surface roughness: (a) spindle speed (b)worktable feed rate (c)grinding depth on surface roughness

3.3 Grinding surface defects

3.3.1 Ground surface morphology

The ground surface defects for KDP crystal samples are mainly in the form of plastic grinding cracks, brittle flaking pits, surface pollution and burn cracks. As shown

in Fig. 5, the pictures of ground surfaces under the grinding depth of 20μm, 10μm and 2μm, taken by the optical microscope. The grinding marks are reasonably clean, with visible plastic grinding crack. Brittle flaking pits, perhaps caused by the crossover of micro cracks, can also be observed. No obvious grinding burn cracks were observed. Under grinding depth 20μm,there were more brittle flaking pits on the sample surface and bigger surface roughness (R_a=0.312) than the other two samples. They has similar surface roughness under the grinding depth 10μm (R_a=0.274) and 2μm (R_a=0.252), however, the density of brittle flaking pits was relatively high for grinding depth 2μm, whilst the depths of the brittle flaking pits were obviously shallower than those under grinding depth 10μm when comparing the surface morphology of the samples.

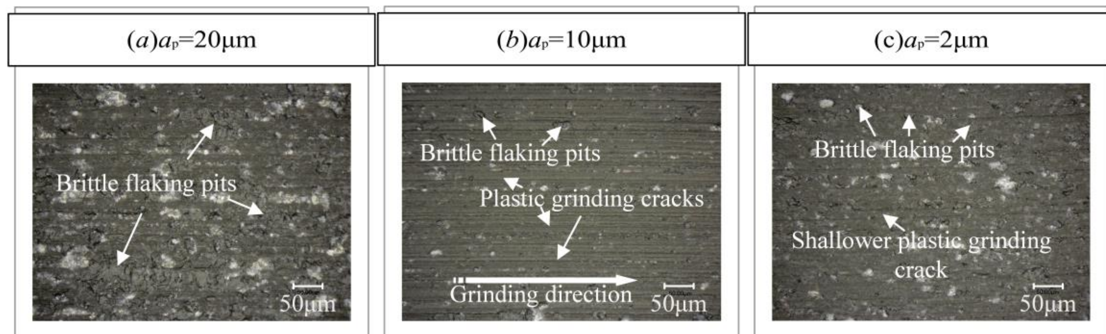

Fig. 5. Grinding surface topography under different grinding depth

3.3.2 Surface impurities embedded

The typical impurities embedded are shown in Fig. 6. The secondary electron image of SEM was used to locate the position of the impurities embedded. As the element weight of the impurities at this position is almost the same as that of the surrounding area, it is identified as a grinding chip embedded, as there was no process fluid applied

to the grinding zone to clean the sample surface, as shown in Fig. 6a. It is suggested that the adoption of an air cleaning nozzle and an abrasive dust collection device would be necessary to reduce or eliminate the chip embedding issue.

A typical abrasive embedded onto the ground surface is shown in Fig.6b. One embedded abrasive was found by scanning electron microscope (SEM). Combined with the back scattered electron imaging, it was found that its element weight distribution was significantly different from the surrounding material. According to further analysis by EDS, it was found that the content of C element of the embedded particle was much higher than the surrounding material. In addition, there was only a little element such as Si, Na, etc. It is thus identified as a abrasive embedding introduced from the abrasive grit pull out from the grinding wheel.

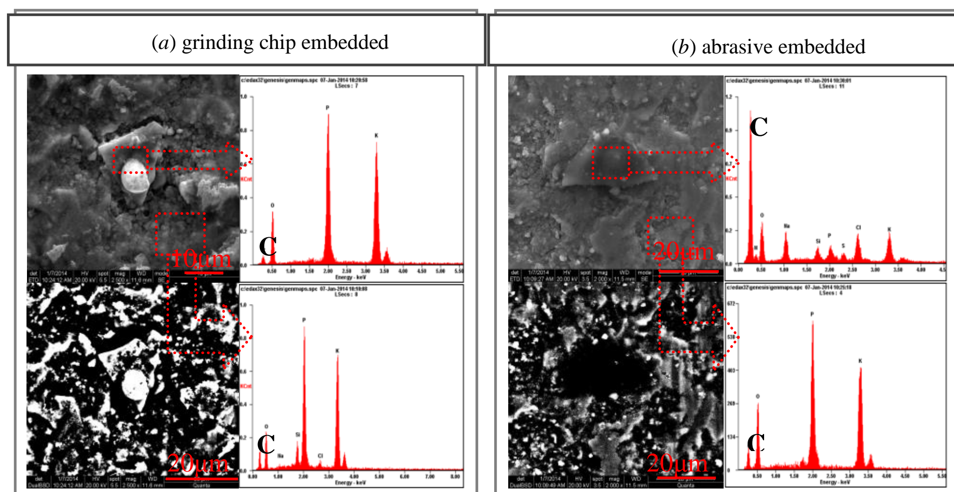

Fig. 6. Typical impurities embedded: (a) grinding chip, (b) abrasive

3.4 Sub-surface damage

As shown in Fig. 7a, the depth of SSD is less than 18μm for the sample ground with grinding depth of 20μm. Grinding marks and flaking pits are very shallow at 2μm depth beneath the original top surface; there are a large number of herringbone and arc-shaped micro-cracks at 4μm depth beneath the top surface; at larger depths beneath the surface, the number of herringbone and arc-shaped micro-cracks gradually decreases; At 18μm depth beneath the top surface, no micro-cracks are observed. The SSD is less than 12μm in the case of 10μm grinding depth, as shown in Fig. 7b. The surface damage layer of KDP crystal is less than 6μm in the case of 2μm grinding depth, as shown in Fig. 7c. Comparing the depths of SSD at 4μm beneath the top surface in Fig.7a, 7b, 7c, it shows that the density of herringbone cracks decreases gradually with the reduction of grinding depth. For the cases under grinding depth 10μm and 2μm, although the ground surface roughness R_a are similar, the depths of SSD are significantly different.

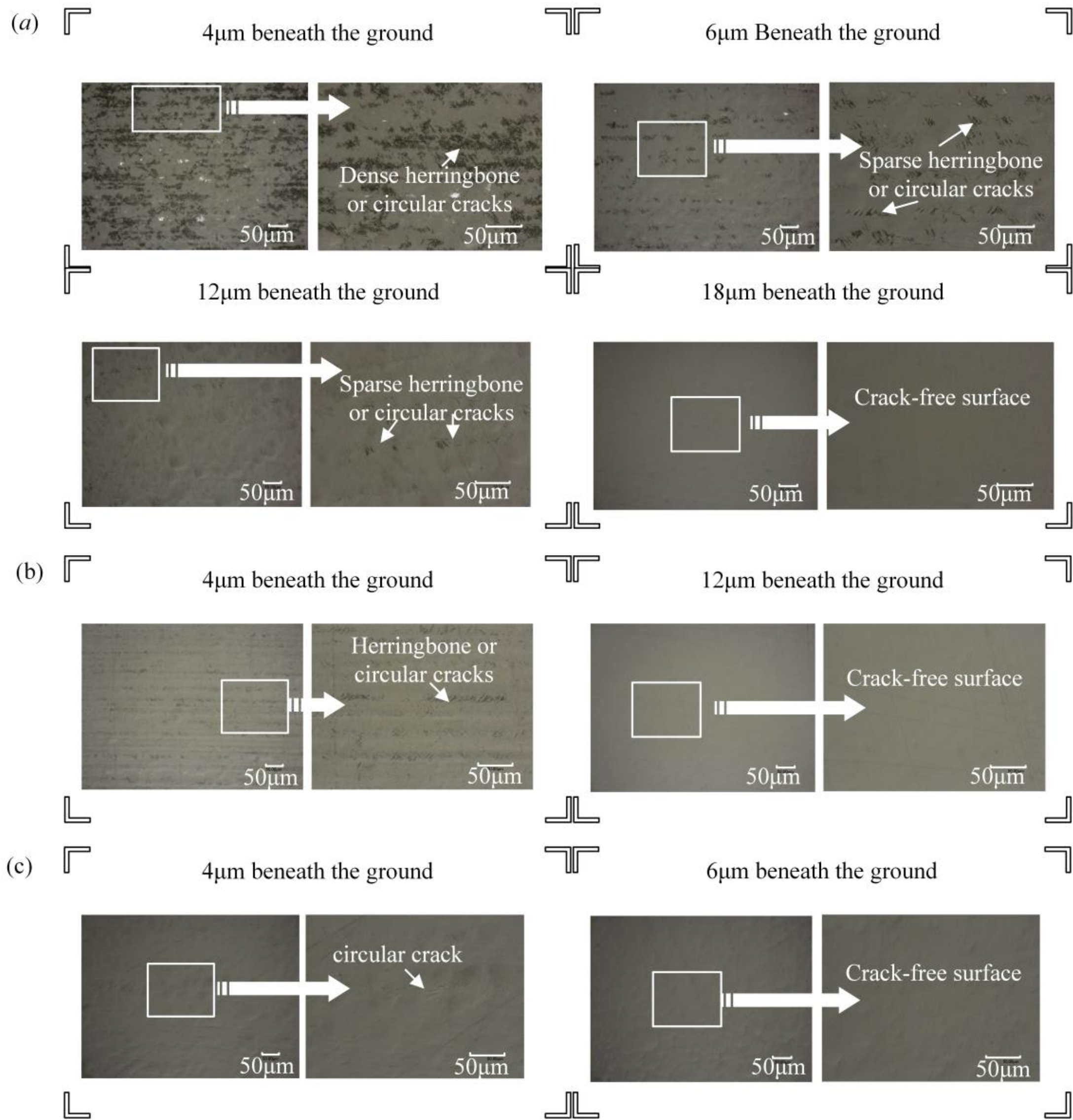

Fig. 7. Observation of sub-surface damages on samples ground obtained using different grinding depths (a) 20μm (b) 10μm and (c) 2μm

4. Discussion

4.1 Grinding direction based on elastic modulus E, Vickers hardness H_V and fracture toughness K_{IC}

According to the variation of elastic modulus E, Vickers hardness H_V and fracture toughness K_{IC}, the 0° or 90° direction on the (001) plane has the high fracture toughness

and high resistance to crack expansion, which is preferable as the grinding direction to reduce the level surface and sub-surface fracture cracks in the grinding process.

4.2 Impurities embedded on machining surface

As KDP is a soft crystal, dusts from the environment, grinding debris and abrasive grits may embed onto the crystal surface causing different types of surface defects, which is a crucial issue for the successful conduction of grinding on this sensitive material. However, in the present research, according to the result of that the machining surface of 20×20mm was magnified 1000times and scanned by line by SEM, it is recognized that the impurities embedding happens just occasionally, only a few(≤3) embedded abrasive grits were found during the whole experimental process, i.e., running 300 grinding passes under different depths of grinding. Individual impurities embedding can be easily picked out and would have little impact on the grinding surface quality.

4.3 Efficiency of the precision grinding method

Wang, et al. studied the deviation of crystal plane orientation, parallelism between opposite surfaces and the sub-surface damages introduced in KDP slicing process. After the final slicing step, the machining allowance, which needs to be removed in the following diamond cutting process, was reported as 544μm [23]. Based on the study of Wang et al. and the experimental results, a grinding process chain is proposed. The process chain is designed to fulfill the task of crystal orientation correction for sliced

KDP work-pieces, removing most of the machining allowance left on the surface after the slicing process, ready for carrying out the following optimal machining procedure. The process chain proposed provides a feasible solution to achieve high process efficiency with satisfactory control of the SSD. The grinding parameters for the process chain are listed in Table 5.

Table 5 Proposed grinding parameter and result

Sequence numbers	Grinding depth (μm)	Worktable feed rate (mm/min)	Spindle speed (r/min)	Surface roughness Ra (μm)	Subsurface damage SSD (μm)
1-25	20	210	7000	0.312	≤18
26-28	10	210	7000	0.274	≤12
29-35	2	210	7000	0.252	≤6

According to the study by Tie et al. [24] investigating the relationship between process parameters and SSD in the single point diamond cutting of KDP crystals, the cutting depth of 16 μm and the feed rate of 20mm/min were suggested for correcting the optical axis of KDP crystal, whilst the surface roughness R_a and SSD obtained in the diamond cutting process are similar to those obtained in the present work using grinding method.

Taking the size of KDP sample (20×20×10mm) used in the present work as an example, for a SPDT process, correcting the axis of KDP crystal spends 34 minutes to remove the 544 μm allowance from the KDP crystal, however, for a grinding method proposed in this work, it only spends 3.4 minutes. The machining efficiency for correcting the axis of KDP crystal would be improved by about ten times using the proposed precision grinding method.

5. Conclusions

The experimental study conducted on a common CNC grinder, using a resin bonded grinding wheel with Ni-P coated diamond abrasives, has proved the feasibility using grinding method to remove the surface material of KDP components with high process efficiency and low surface and sub-surface damages. Main conclusions drawn from this research are as follows:

1. Optimal grinding feed direction, 0°or 90° on the (001) plane, is determined by studying the anisotropic performance of the KDP samples, i.e., variation of the elastic modulus E, Vickers hardness H_V and fracture toughness K_{IC} on the (001) plane.

2. Under the test conditions in this work, impurities embedded on the KDP surfaces were only occasionally observed using SEM, including embedded grinding chips and abrasive grits, but the chance for the impurity embedment is very low, only a few(≤3) embedded abrasive grits were found during the whole experimental process, i.e., running 300 grinding passes under different depths of cut and spindle speeds.

3. The effects of spindle speed, worktable feed rate and grinding depth on the ground surface roughness Ra, have been analyzed and a set of process parameters are proposed for conducting the precision grinding of KDP samples.

4. The machining efficiency using the proposed process parameters, can be improved by nearly ten times, producing nearly the same surface quality (including the

surface roughness R_a≤0.3μm and sub-surface damage≤6μm) as that in the axis fixed phase by SPDT(R_a≤0.2μm, SSD≤6μm).

Acknowledgements

This work was supported by the National Science-Technology Support Plan of China [No. 2012BAF18G00].

References

[1] V. I. Bespalov, V. I. Bredikhin, V. P. Ershov and V. V. Zilberberg, Perspectives for creation of highly effective technology for fabricating KDP and KD*P crystals for ICF, J. Proceedings of SPIE. 3047(1997) 899-902.

[2] J. J. DeYoreo, A. K. Burnham, P. K. Whitman, Developing KH2PO4 and KD3PO4 crystals for the world's most powerful laser, J. International Materials Reviews. 47(2002) 113-152.

[3] J. Borc, K. Sangwal, I. Pritula, E. Dolzhenkova, Investigation of pop-in events and indentation size effect on the (001) and(100) faces of KDP crystals by nano-indentation deformation, J. Materials Science & Engineering A. 708 (2017) 1–10.

[4] Z. Q. Li, P. Q. Ge1, W. B. Bi, T. G. Liu, P. Z. Wang, Y. F. Gao, Coupling stress caused by thermal and slicing force in KDP crystal slicing with fixed abrasive wire saw, J. The International Journal of Advanced Manufacturing Technology. 2018 1-11.

[5] B. A. Fuchs, P. P. Hed, P. C. Baker, Fine Diamond Turning of KDP Crystals, J. Applied Optical. 25(1986) 1733-1736.

[6] D. S. Chen, J. H. Chen, B. R. Wang, A hybrid method for crack-less and high-efficiency ultra-precision chamfering of KDP crystal, J. The International Journal of Advanced Manufacturing Technology. 87(2016) 293-302.

[7] S. F. Wang, C. H. A, F. H. Zhang, J. Wang, X. Y. Lei, J.F. Zhang, An experimental and theoretical investigation on the brittle ductile transition and cutting force anisotropy in cutting KDP crystal, J. International Journal of Machine Tools & Manufacture. 106(2016) 98–108.

[8] G. P. Tie , Y. F. Dai, C. L. Guan, D. C. Zhu, B. Song, Research on full-aperture ductile cutting of KDP crystals using spiral turning technique, J. Journal of Materials Processing Technology. 213(2013) 2137–2144.

[9] W. J. Zong, Z. Q. Li, T, Sun, et al., The basic issues in design and fabrication of diamond-cutting tool for ultra-precision and nanometric madining, J. International Journal of Machine Tools & Manufacture, 50(2010) 411-419.

[10] Y. Namba, M. Katagiri, M. Nakatsuka, Single point diamond turning of KDP inorganic nonlinear crystal for laser fusion, J. The Japan Society for Precision Engineer. 64(1998) 1487-1491.

[11] W. Q. Chen, Y. C. Liang, Y. Z. Sun, et al., Design philosophy of an ultra-precision fly cutting machine tool for KDP crystal machining and its implementation on the structure design, J. International Journal of Advanced Manufacturing Technology. 70(2014), 429–438.

[12] H. Hocheng, H. C. Tseng, M. L. Hsieh, Y. H. Lin, Tool wear monitoring in single-point diamond turning using laser scattering from machined work-piece, J. Journal of Manufacturing Processes. 31 (2018) 405–415.

[13] Y. Namba, Ultra-precision Grinding of Optical Materials for High Power Lasers, J. Proceedings of SPIE. 3244(1998) 320-330.

[14] Q. G. Wang, H. Gao, Q. Z. Zhang, X. S. Cao, R. K. Kang, Experimental Researches on Precision Grinding of KDP Crystal, J. Key Engineering Materials Vols. 359-360(2007) 113-117.

[15] D. S. Chen, J. H. Chen, B. R. Wang, A hybrid method for crackless and high-efficiency ultra-precision chamfering of KDP crystal, J. The International Journal of Advanced Manufacturing Technology. 87 (2016) 293–302.

[16] S. D. Jacobs, Manipulating mechanics and chemistry in precision optics finishing, J. Science and Technology of Advanced Materials. 8(2007) 153-157.

[17] Luo, Z.D., Li, S.J., Anisotropic material mechanics, shanghai jiaotong university,Shanghai, pp. 1994. 5-19.

[18] T. Fang, J.C. Lambropoulos, Micro-hardness and Indentation Fracture of Potassium Dihydrogen Phosphate (KDP), J. Journal of the American Ceramic Society. 85(2002), 174-178.

[19] G. R. Anstis, P. Chantikul, B. R. Lawn, et al., A critical evaluation of indentation techniques for measuring fracture toughness: I, direct crack measurements, J. Journal of the American Ceramic Society. 64(1981), 533-538.

[20] R. Sharma, R. C. Agarwala, V. Agarwala, Development of copper coatings on ceramic powder by electroless technique, J. Applied surface science. 252(2006) 8487-8493.

[21] Y. Zhang, L. C. Zhang, M. Liu, F. H. Zhang, et al., Understanding the friction and wear of KDP crystals by nano-scratching, J. Wear. 332-333(2015) 900–906.

[22] H. N. Li, T. B. Yu, L. D. Zhu, et al., Evaluation of grinding-induced subsurface damage in optical glass BK7. J. Journal of Materials Processing Technology. 229(2016), 785-794.

[23] Q. G. Wang, H. Gao, Z. J. Pei, D. M. Guo, X. J. Teng, An Experimental Investigation on Slicing of Potassium Dihydrogen Phosphate(KDP) Crystal, J. Proceedings of the Institution of Mechanical Engineers Part B Journal of Engineering Manufacture. 227(2013) 890-897.

[24] G. P. Tie, Y. F. Dai, et al., Research on subsurface defects of potassium dihydrogen phosphate crystals fabricated by single point diamond turning technique, J. Optical Engineering. 52(2013) 254-260.